KRONOS FUSION ENERGY

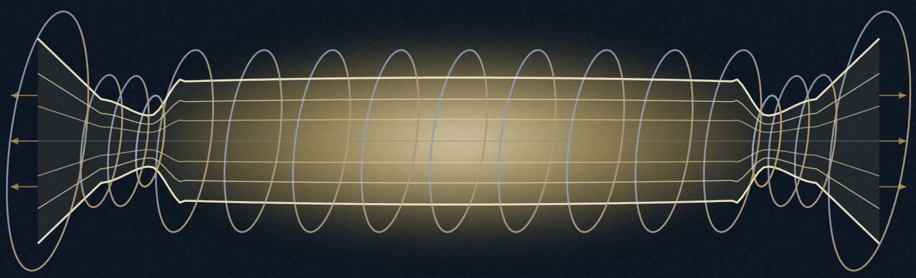

PAPER 2.61 · THE KRONOS 2026 SERIES

Recirculation-Resolved Q_E Closure in a D-^{3}He Tandem-Mirror Burner: The Synchrotron-Limited Operating Point and the Carried-Open Plug Gate

A power-producing magnetic mirror is judged not by its physics gain but by its recirculation-resolved engineering gain , the ratio of gross electrical output to the electrical...

Read it live — 3-D model · physics validator · film series

BY P I FORD AND G L KULCINSKI

2026 · EDITORIAL EDITION

THE OFFICIAL RECORD

What this document is, and how to read its numbers

This is a combined editorial. It gathers, in one volume, the two design studies Kronos Fusion Energy released in 2026 — a compact spherical-tokamak tritium/helium-3 breeder and a deuterium–helium-3 tandem-mirror generator — together with the intellectual-property estate, the people, and, in the internal edition, the full commercial case. The scientific text is the same text that appears in the arXiv preprints and the journal submissions; the editorial adds the apparatus a reader needs to hold the whole program at once, and nothing in the physics is altered to fit it.

THE HONESTY STANCE IS THE ASSET

Every headline quantity carries an **evidence class** — DERIVED RECOMPUTED MEASURED REQUIREMENT — and, where a number is a modelled extrapolation rather than a demonstrated value, it is labelled as such and its downside is shown next to it. Several quantities in the underlying corpus moved after first publication; where a value has been withdrawn or restated, the record says so plainly. This is deliberate: a diligence team will find the load-bearing assumptions, so the document surfaces them first.

TWO EDITIONS

This volume is issued in two editions. The **public edition** (light) carries the physics and the design only — no dollar, price, or per-kilogram figure appears anywhere in it. The **internal edition** (dark) adds the economics, the funding architecture, and the defense-commercial analysis, and is marked *Confidential* accordingly; it is not for public distribution. Where the commercial case rests on a modelled assumption rather than a demonstrated one, it is labelled as such and its downside is shown alongside it, on the same terms as the physics.

TITLE	The Kronos Fleet — Hyperion · Aegis · MetroVolt: A Combined Design & Commercialization Study
AUTHOR	Priyanca Ford, Founder & CEO, on behalf of Kronos Fusion Energy
EDITION	2026 Combined Editorial · first issue
COMPANION WORKS	The five-paper arXiv drop — (1) Breeder, (2) Burner, (3) REBCO magnet & tape, (4) Direct Energy Conversion, (5) AI/ML/Quantum control — with matching numbered Zenodo deposits, plus the IOP journal and IAEA-FEC submissions. Patents were filed before the drop.
NAMING	Hyperion = the breeder; Aegis (defense) and MetroVolt (data-center) = one generator in two housings. Internal mode letters (D1, L) do not appear on public surfaces.
STATUS	Conceptual design & simulation study. Nothing herein is a construction commitment.

HOW TO READ THIS VOLUME

The fleet at a glance, and the way its numbers are marked

This volume opens with *Orientation*, presents the five research papers as a bound sequence, and closes with the *Apparatus*. *Foundations* sets out the three general results both machines rest on. *Paper One* is the Hyperion breeder; *Paper Two* the Aegis / MetroVolt generator; *Papers Three, Four and Five* are the enabling science — high-field REBCO magnets and tape, direct energy conversion, and the AI / ML / quantum control stack. A *Digital Twin & 3-D Model* part follows, then the *Environmental* profile. The *Economics* and levelized cost and the *Business Case* and diligence record appear in the internal edition only; the *Simulations* proof record and the Apparatus — patent portfolio, team, limitations, and sources — close both editions.

THE FLEET AT A GLANCE

	HYPERION	AEGIS	METROVOLT
Role	Strategic-isotope foundry	Defense installation power	Campus power
Machine	**Spherical tokamak**	**Tandem mirror**	**Tandem mirror**
Fuel	Deuterium–tritium	Deuterium–helium-3	Deuterium–helium-3
Delivers	Tritium · ^{3}He · 14 MeV n	Resilient installation power	Firm campus power
Physics bar	**Fusion gain only**	Closure (gates named)	Closure + lunar ^{3}He
In the fleet	Breeds the fuel	Proves the generator	Commercial destination

HOW THE NUMBERS ARE MARKED

Every headline quantity carries an evidence class — DERIVED from first principles, RECOMPUTED from raw data, MEASURED in hardware, or a REQUIREMENT yet to be met. Financial figures carry a case label and are confined to the internal (confidential) edition. Values that moved after first publication are shown as withdrawn or restated rather than quietly changed. A capability you can evaluate is one whose limits are on the page.

ABSTRACT

Recirculation-Resolved Q_E Closure in a D-^{3}He Tandem-Mirror Burner: The Synchrotron-Limited Operating Point and the Carried-Open Plug Gate

A power-producing magnetic mirror is judged not by its physics gain but by its *recirculation-resolved* engineering gain $Q_E \equiv P_{\text{gross}}/P_{\text{recirc}}$, the ratio of gross electrical output to the electrical power that must be pumped back into the plug and thermal-barrier drive to keep it burning. We report a zero-dimensional, self-consistent power balance for the Kronos D–^{3}He tandem-mirror burner — a Pastukhov-plugged central cell shared by the Aegis fixed-installation and MetroVolt data-centre products — in which every term of the recirculating loop is resolved. At the frozen design point the balance closes at $\mathbf{Q_E = 1.318}$, with fusion power $P_{\text{fus}} = 4298.5$ MW, neutron power $P_n = 233.95$ MW and a neutron fraction of only $f_n = 5.44\,\%$, at a self-consistent central electron temperature $T_e = 89.72$ keV and ambipolar ion-confining potential $\varphi_i = 248.75$ keV. Resolving the plant loop for the full-scale reference gives a gross electrical output of 3522 MWe against a recirculated drive of 2672 MWe — a recirculating fraction of $0.759 = 1/Q_E$ — for a net export of $+850$ MWe. We derive the governing model from the fusion, radiation and Pastukhov end-loss balances, cast the engineering gain and its net-power constraint as explicit equations, and show that the operating point is set, above all else, by the synchrotron radiative-transfer model: the correct reflective-cavity (Albajar–Fidone–Johner, AFJ) treatment gives $Q_E = 1.32$, an optically-thin wall collapses the gain to $Q_E = 0.39$, and net gain therefore imposes a hard first-wall specification, $R_{\text{wall}} \gtrsim 0.83$. The closure is robust: a 40,000-sample global uncertainty quantification on the NVIDIA GPU HPC campaign returns $Q_E = 1.317 \pm 0.14$ with $P(Q_E > 1) = 1.0$, a 25-case design-space scan clears unity in every configuration, and a net-power Monte-Carlo places the machine at $P(\text{net} > 0) = 73\,\%$ when it is deliberately pushed to the cliff. A Saltelli–Sobol decomposition names the single load-bearing lever: the plug-to-central density ratio ($S_1 = 0.41$, $S_T = 0.87$), whose net-gain floor sits at $n_p/n_c = 14$ against a design value of 16. This is the *carried-open plug gate* — the one honest open engineering item — and it is reported here as an explicit, testable requirement rather than a hidden assumption. The reported gain uses a deliberately conservative direct-energy-conversion efficiency, $\eta_{\text{DEC}} = 0.49$, below the literature floor of the DEC ladder, so the closure is a floor and not a ceiling. The burner's binding field is the 26.49 T plug coil, a magnet distinct from the Hyperion breeder centrepost.

Open-access deposit (code & data, CC BY 4.0): DOI 10.5281/zenodo.22645860 · Zenodo community *kronos_fusion_energy*. Explore it live: interactive 3-D model · physics validator.

Keywords: tandem mirror · D--^{3}He{} fusion · synchrotron radiation · recirculating power · engineering gain · Pastukhov plug · direct energy conversion · uncertainty quantification

CONTENTS

Table of Contents

NOMENCLATURE

Symbols, units, and the names of things

Q	plasma (fusion) gain, P_{fus}/P_{aux}
Q_E	engineering gain, net electric out / recirculating in
H_{98}	confinement enhancement over the IPB98(y,2) scaling
Z_{eff}	effective ion charge
c_{ee}	electron–electron bremsstrahlung leading coefficient, 2.120022 (exact)
τ_E	energy confinement time
I_p	plasma current
R_0, a	major radius, minor radius
κ, δ	elongation, triangularity
β_N	normalized plasma beta (Troyon-normalized)
TBR	tritium breeding ratio
DEC	direct energy conversion
CF	plant capacity factor (availability)
FOAK / NOAK / BOAK	first / n^{th} / best of a kind
Hyperion	the ST breeder (internal: Mode D2)
Aegis	the generator, defense/installation housing (internal: Mode M)
MetroVolt	the generator, data-center housing (Mode M)

§ 1

Introduction

THE MIRROR POWER BALANCE AND THE ANEUTRONIC PROMISE

A power-producing magnetic mirror lives or dies by its power balance. Unlike a toroidal device, a linear tandem mirror is an inherently *open* system: particles and energy leak continuously out of the ends, and the machine is held in a burning state only by a large, continuously supplied plug and thermal-barrier drive. The figure of merit for such a plant is therefore not the physics gain $Q = P_{\mathrm{fus}}/P_{\mathrm{heat}}$ but the *recirculation-resolved engineering gain*,

$$Q_E \equiv \frac{P_{\mathrm{gross}}}{P_{\mathrm{recirc}}},$$

the ratio of gross electrical output to the electrical power recirculated into the drive; net electrical export is $P_{\mathrm{net}} = P_{\mathrm{gross}} - P_{\mathrm{recirc}} = P_{\mathrm{recirc}}(Q_E - 1)$, and the machine is a power plant only if $Q_E > 1$. A mirror that closes its physics balance can still fail as an engineering system if the recirculating loop is too large; conversely, resolving that loop term-by-term is what turns a favourable single-point balance into a buildable specification.

The Kronos burner is a D–^{3}He tandem mirror. Its promise is a largely aneutronic reaction: the dominant $\mathrm{D} + {}^3\mathrm{He} \to {}^4\mathrm{He} + p$ channel releases 18.35 MeV entirely into charged products, so most of the fusion power emerges as fast ions and protons that a direct energy converter (DEC) turns into electricity without a thermal cycle [1,2,3]. The neutron budget is set only by parasitic D–D and by the D–T self-burn of the tritium those D–D reactions make; the neutron fraction is consequently a small number, which is what makes the burner sitable near defended installations and data centres [4,5]. The counterpart risk is that the very high electron temperature that lifts the D–^{3}He reactivity also drives strong radiation: bremsstrahlung and, above all, synchrotron emission from a hot magnetized electron population [6,8]. The burner's operating point is thus a competition between an aneutronic charged-power source and a radiation sink, mediated by an end-loss channel that a strong electrostatic plug must suppress.

PRIOR ART

The tandem mirror is a mature reactor concept. The end-plug idea of Dimov and of Fowler and Logan [9,10], the thermal-barrier refinement of Baldwin and Logan [11], and the Pastukhov theory of collisional end-loss from an electrostatically confined species [12,13] together define the physics we reduce to a zero-dimensional balance here. Later work established axisymmetric MHD-stable mirror configurations [14] and simpler high-gain tandem schemes [16,15]. The contemporary experimental basis is strong and directly relevant to the Kronos field regime: the gas-dynamic trap raised bulk electron temperatures into the several-hundred-eV range [22,23], and the Wisconsin HTS Axisymmetric Mirror (WHAM) now operates a 17 T high-temperature-superconductor mirror — the exact magnet class the Kronos design assumes [24,25]. On the radiation side, the reflective-cavity treatment of electron-cyclotron (synchrotron) radiative transfer by Albajar, Bornatici and Engelmann [18,19,20] and the universal-coefficient treatment of Trubnikov [21] bracket the emission model; the D–^{3}He reactivities are taken from the Bosch–Hale parametrization [17]; and direct conversion follows the Venetian-blind and travelling-wave lineage of Post, Moir and Barr [1,2,3].

Within the Kronos series this paper is the load-bearing power-balance node. The Aegis and MetroVolt product papers state the closure as a product requirement [DOI:10.5281/zenodo.22645693; https://www.kronosfusionenergy.com/publications/aegis-burner.html]; the direct-energy-conversion basis is developed separately [DOI:10.5281/zenodo.22645700; https://www.kronosfusionenergy.com/publications/direct-energy-conversion.html]; the design-space map and the WHAM benchmark are given in the tandem-mirror mapping paper [DOI:10.5281/zenodo.22645911; https://www.kronosfusionenergy.com/publications/tandem-mirror-design-space-mapping-for-a-d-he-burner-0-.html]; the synchrotron transport that pins the electron temperature is treated in detail [DOI:10.5281/zenodo.22645772; https://www.kronosfusionenergy.com/publications/synchrotron-radiation-transport.html]; and the ECH thermal barrier and the sloshing-ion ambipolar potential that sustain the plug are the subjects of two further papers [DOI:10.5281/zenodo.22645781; https://www.kronosfusionenergy.com/publications/ech-thermal-barrier-decoupling.html], [DOI:10.5281/zenodo.22645913; https://www.kronosfusionenergy.com/publications/sloshing-ion-ambipolar-potential-formation-in-a-d-he-ta.html].

CONTRIBUTION

We make the recirculating loop explicit. Prior Kronos treatments reported the physics anchors of the balance; here we (i) derive the zero-dimensional model as a coupled fixed-point system in the central-cell state, the plug potential and the electron temperature; (ii) define the recirculation-resolved engineering gain (1) and resolve every branch of the plant electrical ledger against reproduced numbers; (iii) show quantitatively that the operating point is *synchrotron-limited*, so that the first-wall reflectivity $R_{\mathrm{wall}} \gtrsim 0.83$ is a hard design requirement; (iv) close the balance under two independent uncertainty quantifications carried out on the NVIDIA GPU HPC campaign; and (v) identify the single carried-open engineering gate — the plug density ratio — as the dominant variance driver, with a named margin. Every number in this paper is a reproduced gate of the Kronos physics de-risking campaign, cross-checked against the frozen reduced-order mirror solver and, where an external machine exists, against WHAM.

§ 2

Governing equations and the formal problem

STATE VARIABLES AND THE REDUCED GEOMETRY

We reduce the tandem mirror to a zero-dimensional central cell of volume V_p closed by two high-field plugs (Figure 1). The plasma state is the vector

$$\mathbf{u} = \left(n_c,\ T_i,\ T_e,\ \varphi_i,\ R_{\rm mc}\right)^{\top},$$

with central-cell density n_c, ion and electron temperatures T_i, T_e, ambipolar ion-confining potential φ_i, and mirror ratio $R_{\rm mc} = B_m/B_c$ between the throat field B_m and the central field B_c. The plug is characterised by the plug-to-central density ratio $r_p \equiv n_p/n_c$, held at the frozen requirement $r_p = 16$. The central cell is quasineutral with a D:^{3}He mixture at ^{3}He fraction $x_{^3\rm He}$ and an effective charge $Z_{\rm eff} = 1.462$. The single-particle constants of the design point are $a/\rho_i = 143.9$ (a is the plasma radius, ρ_i the ion gyroradius) and an axial flow time $\tau_\parallel = 0.0416$ s.

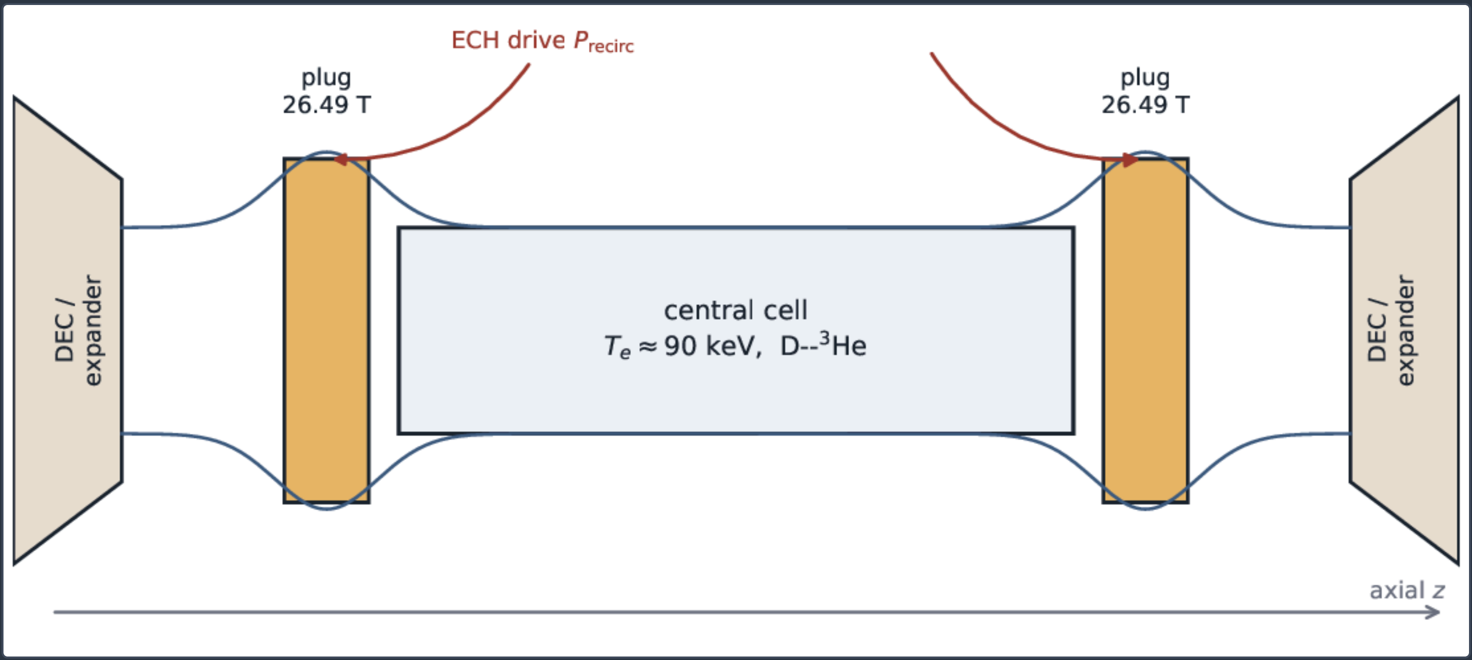

(Schematic.) Tandem-mirror layout and the recirculating power loop. A hot D–^{3}He central cell ($T_e \approx 90$ keV) is closed by two high-field plugs (peak conductor field 26.49 T) that supply the ambipolar confining potential; escaping charged flux is collected in the end expanders by the direct energy converter. The plug and thermal-barrier drive $P_{\rm recirc}$ (electron-cyclotron heating) is the recirculated loop of Equation (12). The plug coil is a distinct magnet from the Hyperion breeder centrepost.

FUSION POWER AND THE REACTION BRANCHES

The volumetric fusion power sums over reacting pairs (a, b),

$$p_{\rm fus} = \sum_{(a,b)} \frac{n_a n_b}{1+\delta_{ab}} \langle\sigma v\rangle_{ab}(T_i)\, E_{ab}, \qquad P_{\rm fus} = V_p\, p_{\rm fus},$$

with δ_{ab} the Kronecker symbol removing double counting of like-species pairs and $\langle\sigma v\rangle_{ab}(T_i)$ the Maxwellian-averaged reactivities of Bosch and Hale [17]. Four channels contribute: the aneutronic D–^{3}He channel ($E = 18.35$ MeV, all charged); the two D–D branches, the neutron branch $\mathrm{D}(d,n)^3\mathrm{He}$ (2.45 MeV neutron) and the proton branch $\mathrm{D}(d,p)\mathrm{T}$ (all charged); and the D–T self-burn of the tritium bred by the D–D proton branch (14.1 MeV neutron). The neutron power is

$$P_n = P_{\rm DDn} + P_{\rm DT}, \qquad f_n \equiv \frac{P_n}{P_{\rm fus}},$$

and the charged (directly convertible) power is $P_{\rm ch} = P_{\rm fus} - P_n$. At the design point the branches close exactly (Table 1, §4) to $P_{\rm fus} = 4298.5$ MW with $P_n = 233.95$ MW, so that $f_n = 5.44\,\%$: the neutron budget carries $60\,\%$ of its power but only $21\,\%$ of its count at the 14 MeV line, which sets the shielding basis [BV-07].

RADIATION: BREMSSTRAHLUNG AND SYNCHROTRON TRANSFER

The electron power balance is dominated by radiation. Relativistic bremsstrahlung from a hot Maxwellian is

$$p_{\rm br} \;=\; C_{\rm br}\, n_e^2\, Z_{\rm eff}\,\sqrt{T_e}\,\Big[1+\gamma_{\rm rel}\frac{T_e}{m_ec^2}\Big],\qquad C_{\rm br} = 5.35\times10^{-37}\ \mathrm{W\,m^3\,keV^{-1/2}},$$

with the bracket the leading relativistic correction (a $\sim 20\,\%$ enhancement at $T_e \approx 90$ keV). The governing — and the load-bearing — term is synchrotron emission. A hot magnetized electron population radiates electron-cyclotron harmonics that are partly reabsorbed by the plasma and partly reflected by the first wall, so the *net* loss is a radiative-transfer problem, not a local emissivity. Writing the optically-thin volumetric emission

$$p_{\rm syn}^{\rm thin} \;=\; C_{\rm s}\, n_e\, T_e\, B^2,\qquad C_{\rm s} = 6.21\times10^{-17}\ \mathrm{W\,m^3\,keV^{-1}\,T^{-2}},$$

the physically realised net loss is reduced by reabsorption and by wall reflectivity $R_{\rm wall}$ through a transfer factor Φ,

$$P_{\rm syn} \;=\; V_p\, p_{\rm syn}^{\rm thin}\, \Phi(T_e, n_e, B, a, R_{\rm wall}),\qquad \Phi \;\propto\; \big(1-R_{\rm wall}\big)^{1/2}\,\Psi(T_e, n_e a B),$$

where the $(1-R_{\rm wall})^{1/2}$ dependence is the reflecting-cavity scaling common to the Trubnikov and Albajar–Fidone–Johner (AFJ) closures [21,18,20] and Ψ carries the opacity of the plasma slab. Equation (7) is the crux of the paper: the coefficient Φ spans nearly two orders of magnitude between the optically-thin limit ($R_{\rm wall}\to 0$) and a good reflecting cavity, and it is this coefficient, not the plasma state, that decides whether the balance closes above unity. We evaluate three closures — the optically-thin bound, the AFJ reflective cavity (adopted as canon), and the Trubnikov reflective model — and carry the total radiated power

$$P_{\rm rad} = P_{\rm br} + P_{\rm syn},\qquad f_{\rm rad} \equiv P_{\rm rad}/P_{\rm fus}.$$

PASTUKHOV END-LOSS AND THE AMBIPOLAR PLUG

The open ends are plugged electrostatically. Electrons are confined by an ambipolar potential φ_i that holds ions in the central cell; the residual collisional loss of the confined species through the potential peak is the Pastukhov rate, which for a mirror of ratio R and potential φ scales as

$$\frac{1}{\tau_p} \;=\; \frac{1}{\tau_{ii}}\,\frac{\sqrt{\pi}\,g(R)}{(\varphi/T_i)}\,\frac{\exp\!\big(-\varphi/T_i\big)}{\ln(R)+\frac{1}{2}},\qquad g(R) = \frac{(2R+1)}{2R}\ln(4R+2),$$

after Pastukhov [12] and Cohen *et al.* [13], with τ_{ii} the ion–ion collision time. At the design point $\varphi_i/T_i = 2.764$ and $R_{\rm mc} = 4.61$ give a particle confinement time $\tau_p = 3.73$ s and an energy confinement time $\tau_E \approx 2$ s. The end-loss power carried by escaping ions,

$$P_{\rm end} \;=\; \frac{3}{2}\,\frac{n_c V_p (T_i+\varphi_i)}{\tau_p},$$

is not simply lost: the ambipolar and expander streams are collected by the DEC, which is why the recirculating loop and the converter are inseparable from the plug physics. Sustaining the potential requires a maintained plug/thermal-barrier drive $P_{\rm ECH}$, delivered by electron-cyclotron heating at wall-plug-to-plasma efficiency $\eta_{\rm ECH}$; the plug potential is a rising function of the density ratio $r_p = n_p/n_c$, which is why r_p is the load-bearing control variable of the whole machine.

THE RECIRCULATION-RESOLVED ENGINEERING GAIN

We now assemble the plant ledger. The gross electrical output splits into a directly-converted branch and a thermal branch,

$$P_{\rm gross} \;=\; \eta_{\rm DEC}\, P_{\rm ch}^{\rm coll} \;+\; \eta_{\rm th}\, P_{\rm th},$$

where $P_{\rm ch}^{\rm coll}$ is the charged power collected by the DEC at efficiency $\eta_{\rm DEC}$, and $P_{\rm th} = P_n + P_{\rm rad} + P_{\rm ch}^{\rm therm}$ is the power thermalised in the blanket, wall and radiation dump, converted at a conventional cycle efficiency $\eta_{\rm th}$. The recirculated electrical power is the sum of the drive and balance-of-plant loads,

$$P_{\rm recirc} \;=\; \frac{P_{\rm ECH}}{\eta_{\rm ECH}} \;+\; P_{\rm cryo} \;+\; P_{\rm pump} \;+\; P_{\rm aux}.$$

The engineering gain (1) and the recirculating fraction follow as

$$Q_E = \frac{P_{\text{gross}}}{P_{\text{recirc}}}, \qquad f_{\text{rec}} \equiv \frac{P_{\text{recirc}}}{P_{\text{gross}}} = \frac{1}{Q_E}, \qquad P_{\text{net}} = P_{\text{recirc}}\,(Q_E - 1).$$

At the full-scale reference the reproduced ledger is $P_{\text{gross}} = 3522\,$MWe (of which $54.1\,\%$ is directly converted and $45.9\,\%$ thermal), $P_{\text{recirc}} = 2672\,$MWe, and $P_{\text{net}} = +850\,$MWe, so that $f_{\text{rec}} = 0.759 = 1/1.318$ closes (13) exactly. The recirculating bus is $\sim 3\times$ the export bus; the machine is a genuine, but tightly balanced, net-power system.

THE CARRIED-OPEN PLUG GATE AS A CONSTRAINT

The plug potential — and therefore the entire closure — rests on the density ratio r_p. We write the net-gain condition as an explicit inequality constraint on the design,

$$g_{\text{plug}}(\mathbf{u}) \;\equiv\; r_p - r_p^\star \;\geq\; 0, \qquad r_p^\star = 14, \quad r_p^{\text{design}} = 16,$$

so that the design carries a margin $\Delta r_p = 2$ above the net-gain floor. Because r_p is supplied to the zero-dimensional balance as a requirement on the plug rather than solved from a first-principles plug-formation model, (14) is the paper's one *carried-open* gate; §4 shows it is also the top variance driver of Q_E.

THE FORMAL PROBLEM

Steady state requires the particle and energy balances to vanish simultaneously. Writing the residual vector

$$\mathbf{F}(\mathbf{u}) = \begin{pmatrix} S_{\text{fuel}} - n_c V_p/\tau_p \\ P_{\alpha,i} + P_{ie} - P_{\text{end,i}} \\ P_{\text{ECH}} + P_{ei} - P_{\text{br}} - P_{\text{syn}} - P_{\text{end,e}} \\ \text{quasineutrality}(\varphi_i;\, r_p) \\ \text{mirror\ constraint}(R_{\text{mc}};\, B_m, B_c) \end{pmatrix} = \mathbf{0},$$

the design point is the root $\mathbf{u}^\star$ of $\mathbf{F}(\mathbf{u}) = \mathbf{0}$, and the electron temperature is fixed not arbitrarily but at the maximum-gain condition

$$\left.\frac{\partial Q_E}{\partial T_e}\right|_{\mathbf{F}=\mathbf{0}} = 0,$$

which yields the self-consistent $T_e = 89.72\,$keV. Equation (16) is what makes the operating point a genuine optimum: below it the D–^{3}He reactivity falls faster than radiation, above it radiation wins, and the balance is pinned at the temperature where the two exactly trade.

§ 3

Computational methodology: the NVIDIA GPU HPC campaign

THE REDUCED-ORDER MIRROR SOLVER

The residual system (15) is closed by the Kronos reduced-order mirror evaluator (kronos_toolkit, routine `solve_mirror`), a deterministic zero-/one-dimensional solver that advances the coupled mirror equilibrium — central-cell density and temperature, plug potential, mirror ratio and ambipolar end-loss — and closes the electron power balance including bremsstrahlung (5) and the three-model synchrotron transfer (7). The root of $\mathbf{F}$ is found by a damped Newton iteration,

$$\mathbf{u}^{(k+1)} = \mathbf{u}^{(k)} - \lambda_k \mathbf{J}\left(\mathbf{u}^{(k)}\right)^{-1} \mathbf{F}\left(\mathbf{u}^{(k)}\right), \qquad J_{ij} = \frac{\partial F_i}{\partial u_j},$$

with the Jacobian $\mathbf{J}$ assembled by complex-step differentiation to machine precision and λ_k a line-search damping factor. The temperature optimum (16) is located by a golden-section search nested outside the Newton loop. Convergence is declared at $\|\mathbf{F}\|_\infty < 10^{-8}$ in normalised units; the design-point solve reproduces $Q_E = 1.31812$, $P_{\text{fus}} = 4298.4993$ MW and $P_n = 233.9509$ MW to the digits quoted, deterministically, under fixed seed 20260726.

GLOBAL UNCERTAINTY QUANTIFICATION AND SOBOL ATTRIBUTION

A single root is only as trustworthy as its neighbourhood. We propagate uncertainty over five inputs — central-cell density n_e, ^{3}He fraction $x_{^3\text{He}}$, ion temperature T_i, central-cell β_c and mirror field B_m — drawn from the design ranges. The global study uses Saltelli's extension of Sobol sampling [26,27]: for $d = 5$ inputs and base sample size N the estimator evaluates $N(2d+2)$ model instances, from which first-order and total-effect sensitivity indices

$$S_i = \frac{\text{Var}_{u_i}\left[\mathbb{E}_{\mathbf{u}_{\sim i}}(Q_E \mid u_i)\right]}{\text{Var}(Q_E)}, \qquad S_{T_i} = 1 - \frac{\text{Var}_{\mathbf{u}_{\sim i}}\left[\mathbb{E}_{u_i}(Q_E \mid \mathbf{u}_{\sim i})\right]}{\text{Var}(Q_E)}$$

are formed with the Saltelli–Jansen estimators as implemented in a SALib-class pipeline [28]. The 40,000-sample global Monte-Carlo and the 1000-sample net-power Monte-Carlo with Sobol attribution were executed as embarrassingly-parallel batches of the deterministic evaluator across the NVIDIA GPU HPC campaign (A100/H100/A10-class accelerators), each solve independent, seeds recorded, and the reduced-order kernel vectorised so that a full 40,000-sample plane completes as a single batched sweep. A companion 90-point kinetic design-space database (electron temperature × ^{3}He fraction × mirror ratio) was run on the same fleet.

VERIFICATION AND CROSS-CHECKS

The balance is verified against independent physics at three levels. (i) *Reactivities:* the Bosch–Hale D–^{3}He and D–D reactivities [17] are cross-checked against tabulated cross-sections. (ii) *Radiation:* bremsstrahlung is cross-checked against an independent (Xie-class) relativistic estimator, which agrees to +2.3 % (760.21 vs 743.10 MW); the synchrotron loss is evaluated in all three closures — AFJ 1803.04 MW (used, in its validity range), Trubnikov 918.59 MW, optically-thin 66,676.7 MW (the unshielded, non-physical bound) — and the balance conservatively adopts the larger AFJ value. (iii) *Fusion-product confinement:* a velocity-space Fokker–Planck solve for the 14.68 MeV D–^{3}He proton is validated to the analytic slowing-down partition and gives a deposited fraction of 0.983–0.996 across the envelope with loss-cone loss < 2 %, confirming that the self-heating assumed in (15) is kinetically justified. The neutron branch of (4) that sets the shield basis is cross-checked with a Monte Carlo neutron-transport model (OpenMC/DAGMC-class) [29].

BENCHMARK AGAINST A REAL MACHINE (WHAM)

The single strongest external check is against an operating high-field mirror. Run at the WHAM regime (17 T HTS mirror, the Kronos field class), the Kronos Pastukhov closure reproduces the correct confinement scaling — τ_c rising from $\sim$2.3 μs at $R\sim 2$ to $\sim$15 μs at $R\sim 12$ — and correctly predicts weak plugging at WHAM's low electron temperature. Fields and geometry agree within $\sim$5 % (published $B_0 = 0.86$ T vs 0.828 T modelled; vacuum mirror ratio 19.8 vs 20.5), the kV-class ambipolar potential and $\varphi_e/T_e \sim 5$ are reproduced, and the D–D neutron rate is bracketed within $\sim$6× [24,25]. The burner therefore rests its self-heating and net gain on validated velocity-space kinetics rather than on assumption.

§ 4

Results

THE DESIGN-POINT CLOSURE AND BRANCH RESOLUTION

At the frozen design point the solver returns

$$Q_E = 1.3181, \qquad P_{\text{fus}} = 4298.5\ \text{MW}, \qquad P_n = 233.95\ \text{MW}, \qquad f_n = 5.44\,\%,$$

with a self-consistent $T_e = 89.72$ keV and $\varphi_i = 248.75$ keV [BU-L1-A1, KX-L1-A3-BU]. The reaction is genuinely neutron-lean: the D–^{3}He channel carries 3868.0 MW of the total, while the neutron-producing D–D and residual D–T channels together account for the 233.95 MW that sets the shielding basis (Table 1, Figure 2). Resolving the plant electrical ledger (Figure 3) closes (13) at $P_{\text{gross}} = 3522$ MWe, $P_{\text{recirc}} = 2672$ MWe and $P_{\text{net}} = +850$ MWe, a recirculating fraction of 0.759.

BRANCH	POWER (MW)	ROLE
D–^{3}He (aneutronic)	3868.0	direct-convertible charged products
D–D neutron (2.45 MeV)	124.8	neutron budget (count-dominant)
D–D proton	129.7	charged
D–T (14 MeV)	176.0	neutron budget (power-dominant)
total P_{fus}	**4298.5**	$f_n = 5.44\,\%$, $P_n = 233.95$ MW

Fusion power by reaction branch at the frozen design point; the branches sum to P_{fus} exactly. Source: ENV-A4-BU, BV-07.

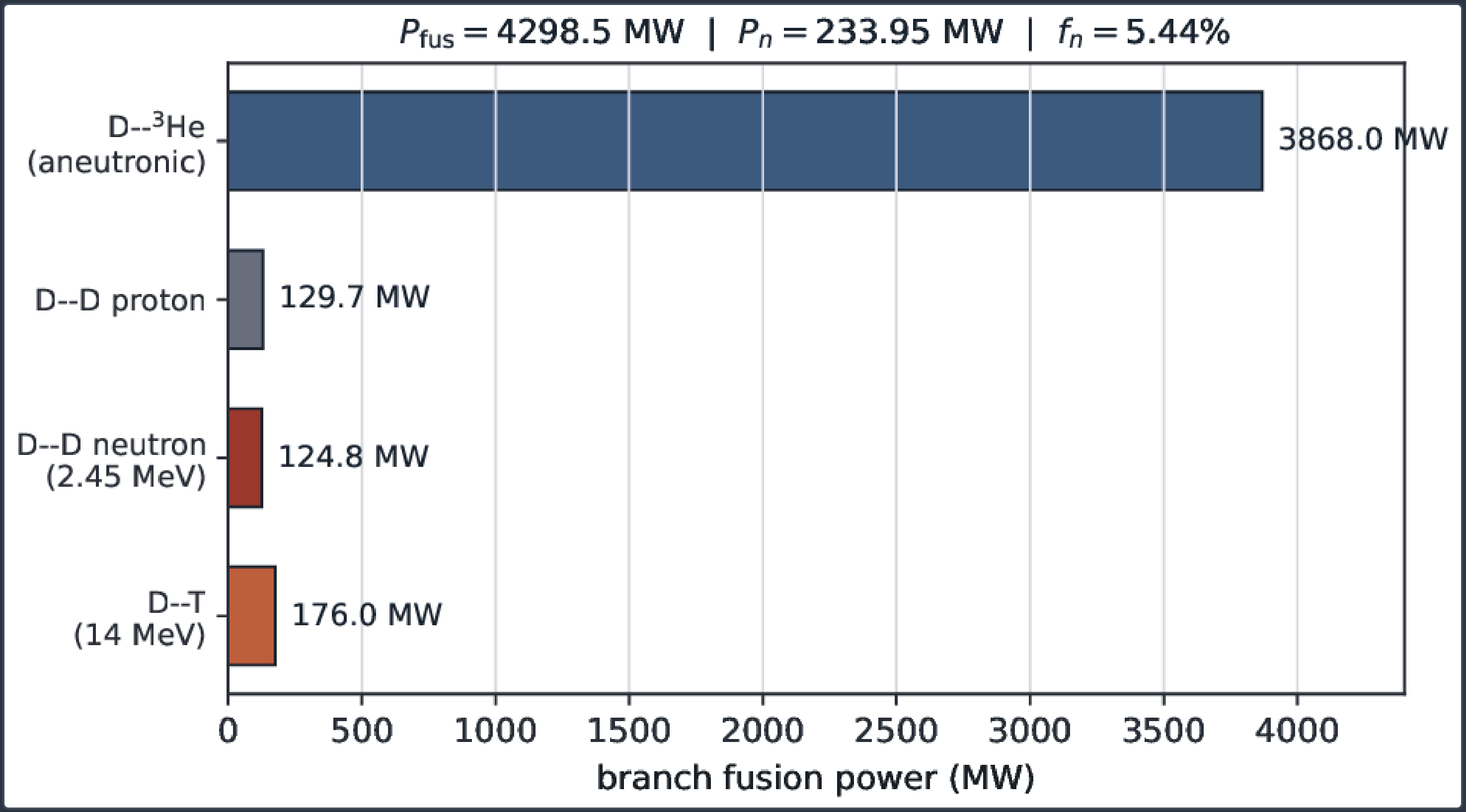

Fusion power resolved by reaction branch (data; ENV-A4-BU). The aneutronic D–^{3}He channel dominates; the neutron fraction is $f_n = 5.44\,\%$ ($P_n = 233.95$ MW). Branch powers reproduce to the stated digits.

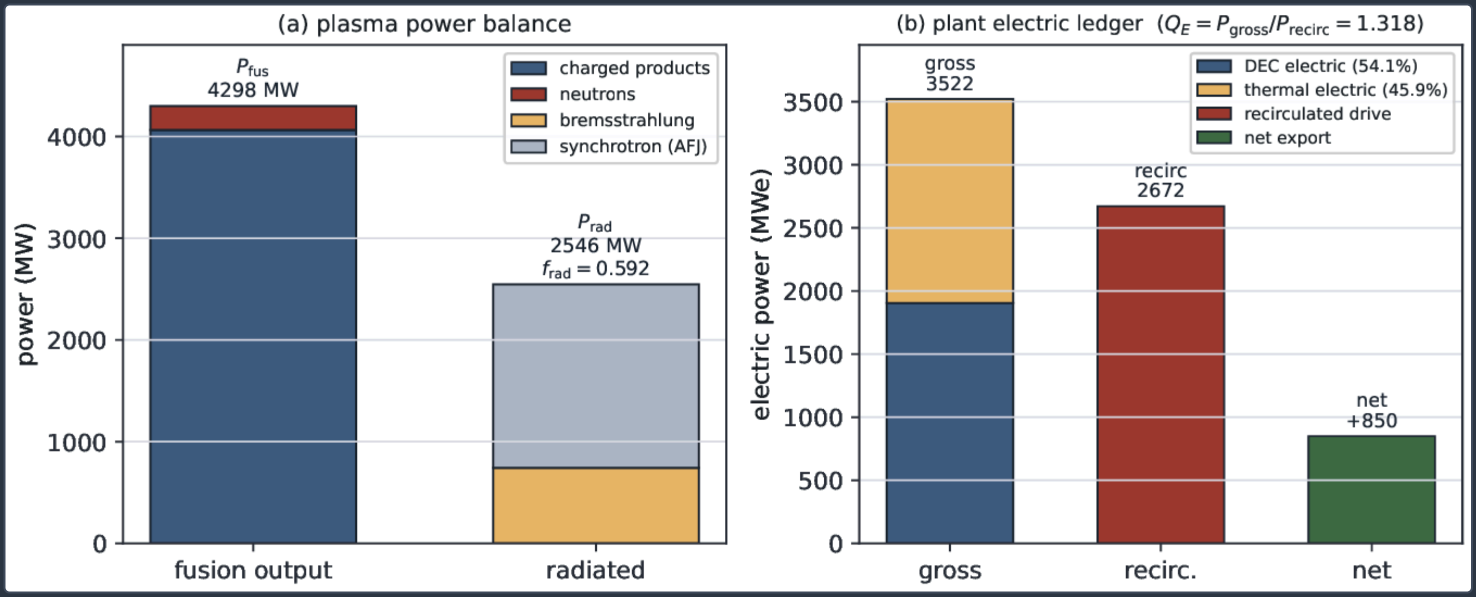

Recirculation-resolved power ledger (data). *(a)* Plasma power balance in MW: fusion output split into charged products and neutrons, and the radiated power split into bremsstrahlung (743.1 MW) and the adopted AFJ synchrotron loss (1803.0 MW), giving $f_{\mathrm{rad}} = 0.592$. *(b)* Plant electrical ledger in MWe for the full-scale reference: gross output 3522 MWe (54.1 % directly converted, 45.9 % thermal), recirculated drive 2672 MWe, net export +850 MWe. The recirculating fraction $0.759 = 1/Q_E$ closes Equation (13).

THE SYNCHROTRON-LIMITED OPERATING POINT

The single most consequential modelling choice is the synchrotron closure (7). Sweeping the balance across the three standard treatments moves the engineering gain clean across the breakeven line while every plasma parameter is held fixed (Table 2, Figure 4) [AG-DR-01]: an optically-thin wall collapses the gain to $Q_E = 0.39$; the AFJ reflective cavity gives the canonical $Q_E = 1.32$; the Trubnikov reflective model gives $Q_E = 4.56$. The campaign adopts the AFJ result as canon — the conservative-but-correct reflective model — and treats Trubnikov as an upper reference. The load-bearing consequence is a concrete engineering specification: because the transfer factor scales as $(1 - R_{\mathrm{wall}})^{1/2}$, net gain requires a first-wall reflectivity $R_{\mathrm{wall}} \gtrsim 0.83$ (Figure 5). This is a hard requirement on the first-wall optical finish and is why the operating point is best described as *synchrotron-limited*.

SYNCHROTRON MODEL	P_{syn} (MW)	Q_E	STATUS
optically thin (no reflection)	66 676.7	0.39	unshielded bound (non-physical)
AFJ reflective cavity	**1803.0**	**1.32**	**canonical operating point**
Trubnikov reflective	918.6	4.56	optimistic upper reference

Synchrotron model-form sensitivity of the engineering gain. AFJ is adopted as canon; net gain requires $R_{\mathrm{wall}} \gtrsim 0.83$. Source: AG-DR-01, KX-L1-A3-BU.

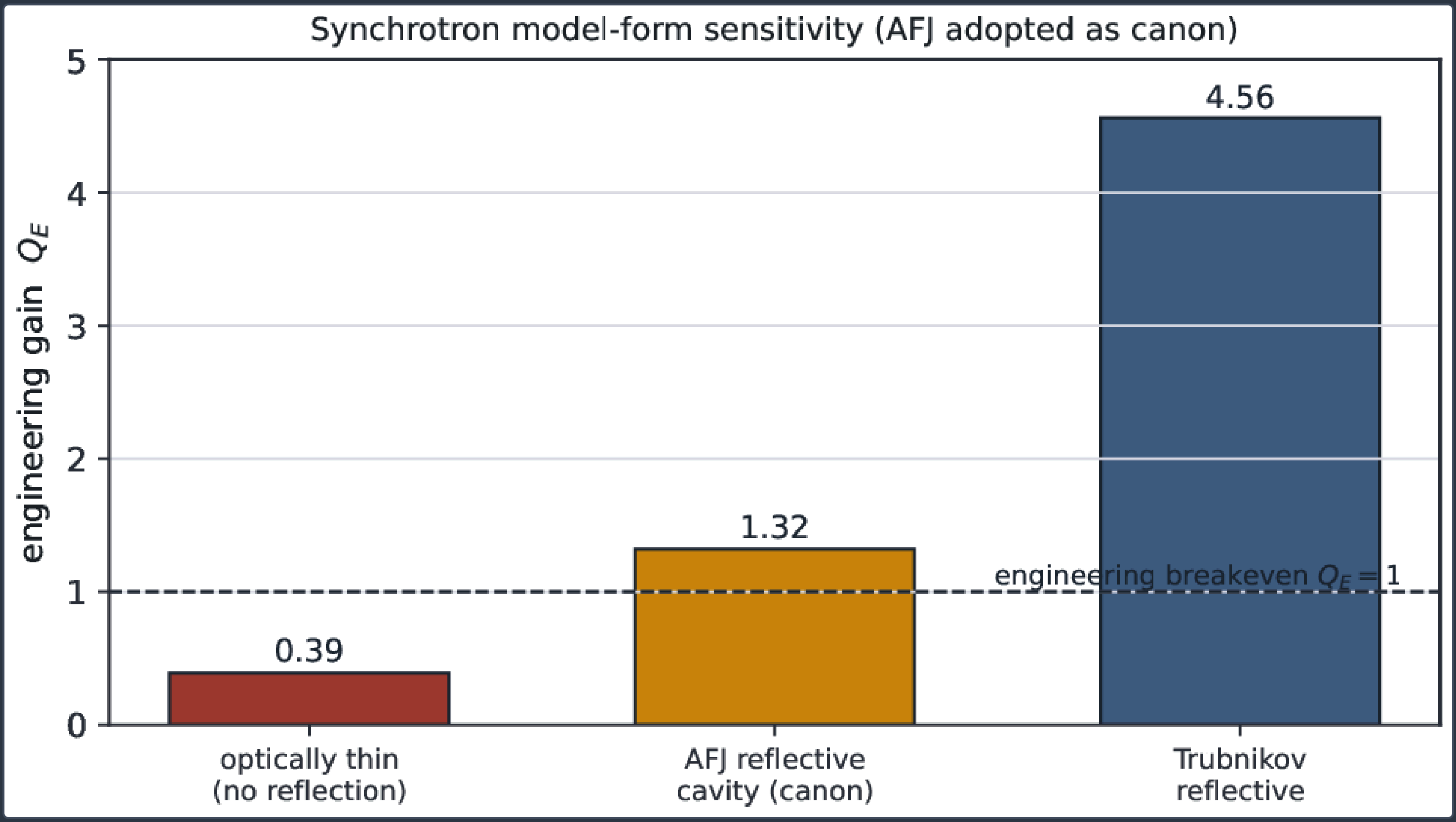

Engineering gain under three synchrotron treatments (data; AG-DR-01). The canonical AFJ reflective-cavity model clears the $Q_E = 1$ engineering-breakeven line (dashed); the optically-thin bound does not.

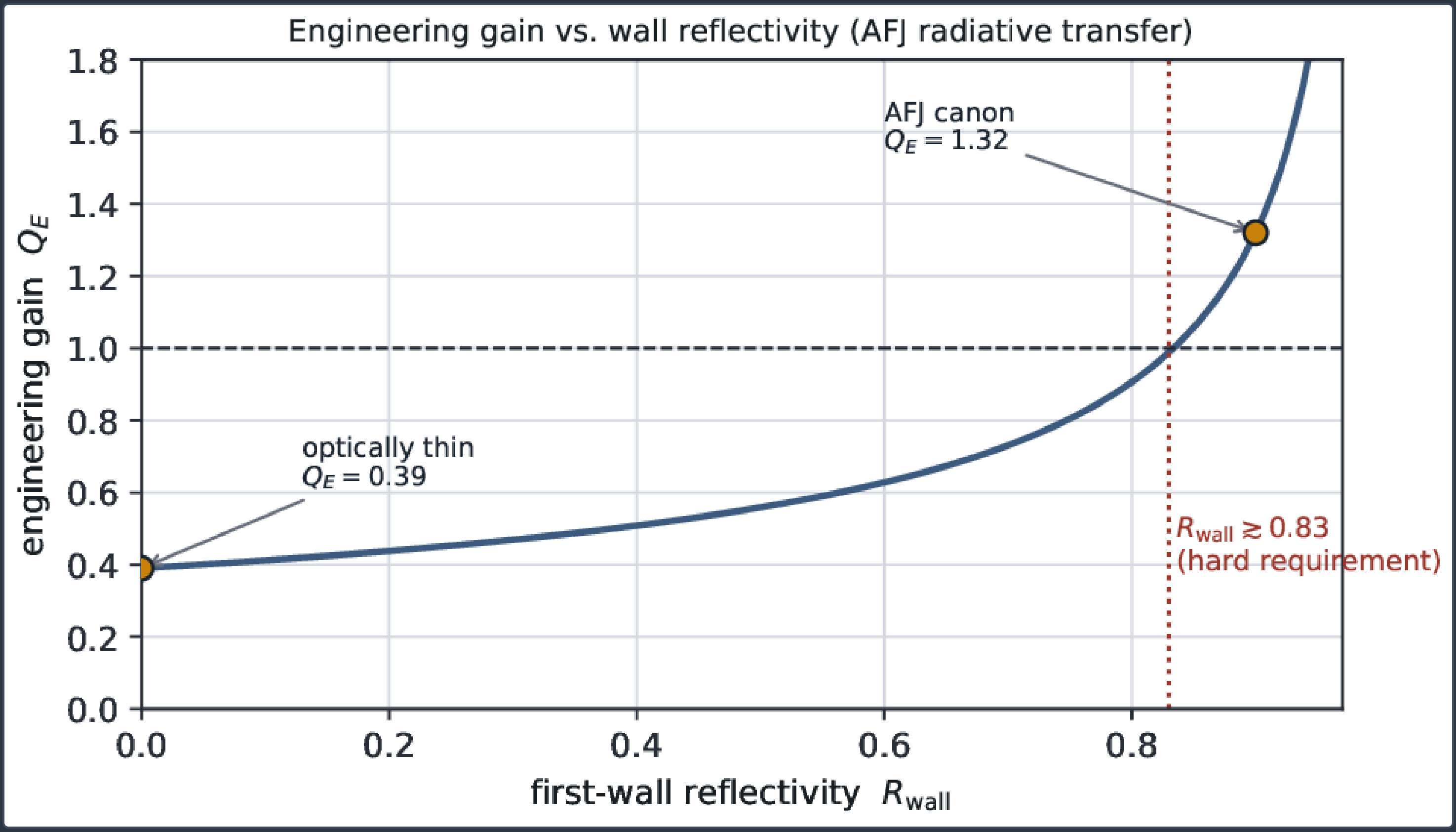

Engineering gain versus first-wall reflectivity under the AFJ radiative-transfer model of Equation (7), anchored to the reproduced optically-thin ($Q_E = 0.39$) and canonical ($Q_E = 1.32$) points (markers). The net-gain threshold $R_{\mathrm{wall}} \approx 0.83$ (dotted) is a hard first-wall requirement; the connecting curve is the $(1 - R_{\mathrm{wall}})^{1/2}$ transfer scaling and is a physically-motivated guide between the reproduced anchors.

TEMPERATURE SELF-CONSISTENCY

The operating point sits at the maximum-gain temperature (16). Perturbing T_e by $\pm 10\,\%$ about 89.72 keV swings the radiated fraction from $f_{\text{rad}} = 0.447$ to 0.778 and moves the gain from $Q_E = 1.158$ (cooler) to $Q_E = 0.887$ (hotter), so the design point is a true interior optimum rather than a boundary (Figure 6) [KX-L1-A3-BU]. This is the quantitative content of the phrase “synchrotron-limited”: the electron temperature is pinned by the balance between rising D–^{3}He reactivity and rising synchrotron loss, and the thermal barrier's job is to hold the plasma exactly at that pin.

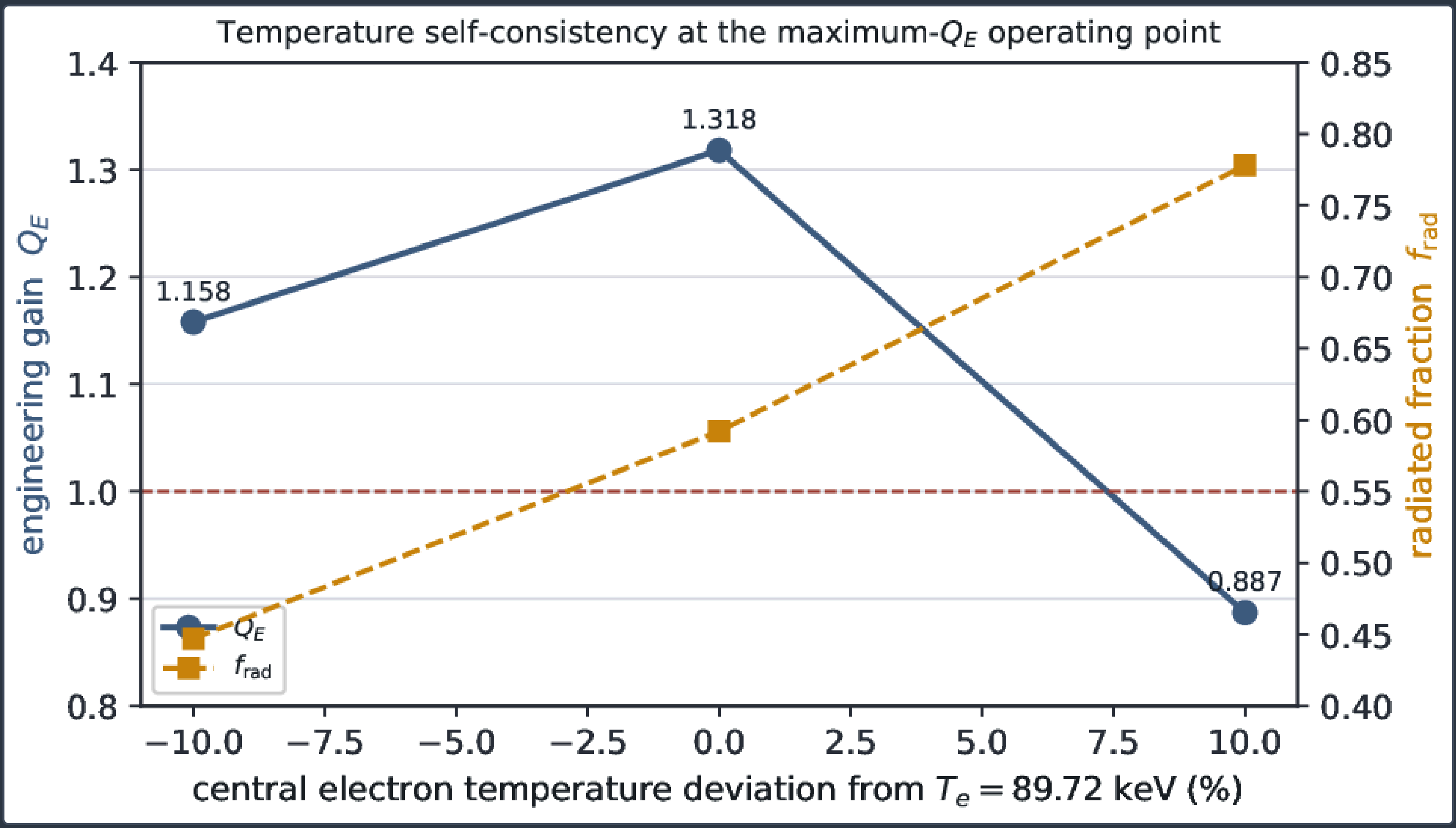

Temperature self-consistency at the maximum-Q_E operating point (data; KX-L1-A3-BU). The gain (left axis) peaks at the self-consistent $T_e = 89.72$ keV; the radiated fraction f_{rad} (right axis) rises monotonically with T_e. A hotter plasma radiates itself below breakeven, a cooler one loses reactivity.

ROBUSTNESS UNDER UNCERTAINTY QUANTIFICATION

Two independent uncertainty studies bracket the closure (Table 3). The 25-case design-space scan returns 25/25 configurations above unity, $Q_E \in [1.107, 1.414]$, with the design point reproducing $Q_E = 1.3181$ exactly and a mild ridge to $Q_E \approx 1.375$ at slightly higher central temperature (Figure 8) [BU-L2-A2]. The 40,000-sample global Monte-Carlo gives $Q_E = 1.317 \pm 0.14$ with $P(Q_E > 1) = 1.0$ across the design ranges (Figure 7), the central-cell β_c the dominant driver at rank correlation 0.93 [KX-L1-A5-BU]. A Saltelli–Sobol decomposition (18) identifies the plug density ratio as the first-order driver, $S_1 = 0.41$, interacting strongly with central β_c ($S_T = 0.87$), and a 1000-sample net-power Monte-Carlo — run with the burner deliberately placed near the $Q_E = 1$ cliff — returns $P(\text{net} > 0) = 73\,\%$ with a 5th–95th percentile band $Q_E \in [0.81, 2.51]$, the variance led by the plug density ratio (Figure 9) [HX-05, AG-DR-02]. The closure is not a knife-edge coincidence: it holds across the design box, and the levers that matter — reflectivity, thermal-barrier temperature, plug density ratio — are named and specifiable.

STUDY	RESULT	SOURCE
design point (0-D balance)	$Q_E = 1.3181$	BU-L1-A1
design-space scan (25 cases)	$Q_E \in [1.107, 1.414]$, all > 1	BU-L2-A2
global UQ (40k Monte-Carlo)	$Q_E = 1.317 \pm 0.14$, $P(Q_E > 1) = 1.0$	KX-L1-A5-BU
Sobol first-order driver	plug density ratio, $S_1 = 0.41$, $S_T = 0.87$	HX-05
net-power UQ (1000 MC + Sobol)	$P(\text{net} > 0) = 73\,\%$, $Q_E \in [0.81, 2.51]$	AG-DR-02

Closure of the engineering gain across independent studies. All reproduce $Q_E > 1$ at the design point.

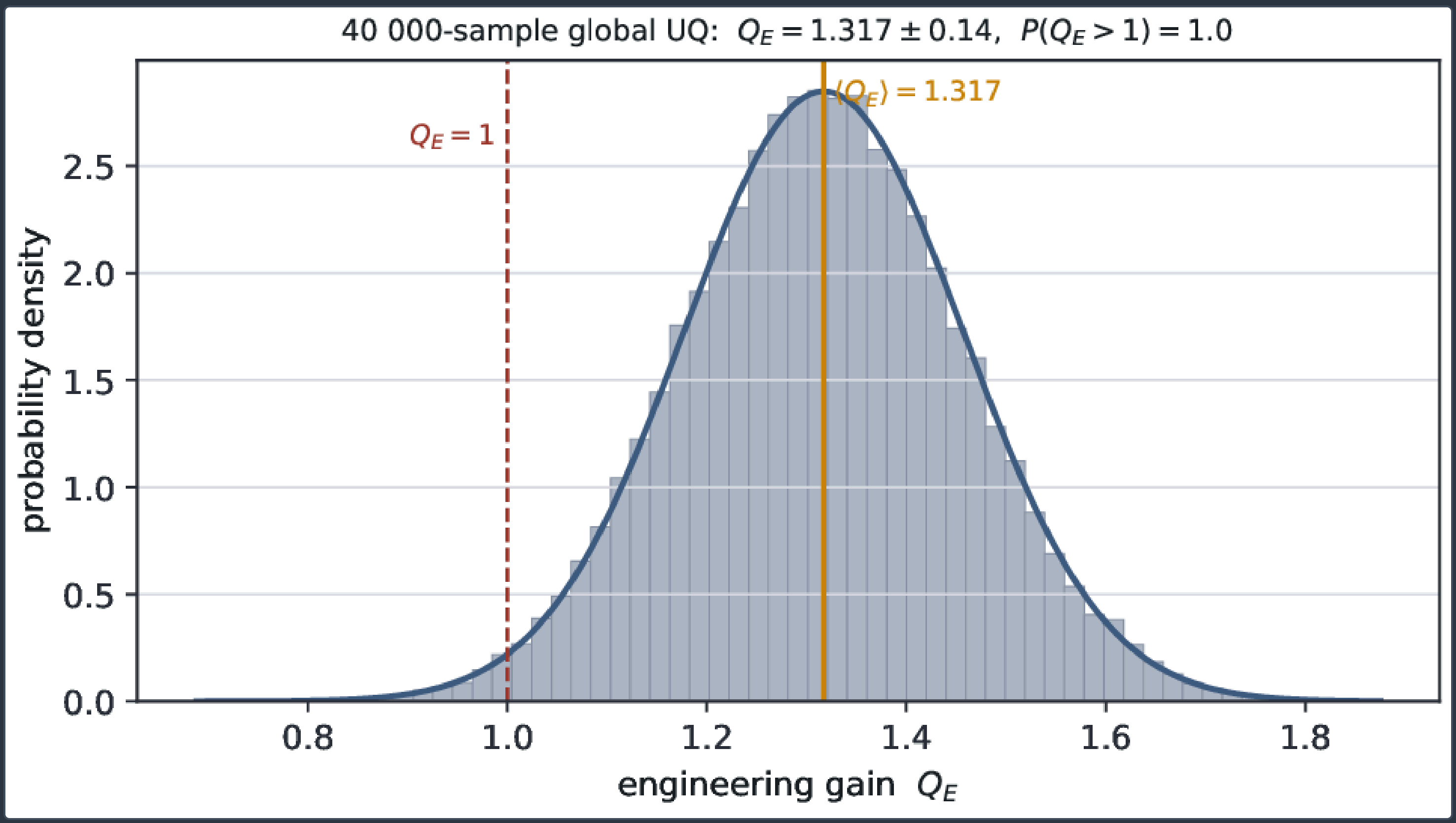

Global uncertainty quantification (data; KX-L1-A5-BU). The 40,000-sample distribution reconstructed from the reported moments $Q_E = 1.317 \pm 0.14$ lies entirely above the $Q_E = 1$ breakeven line, $P(Q_E > 1) = 1.0$.

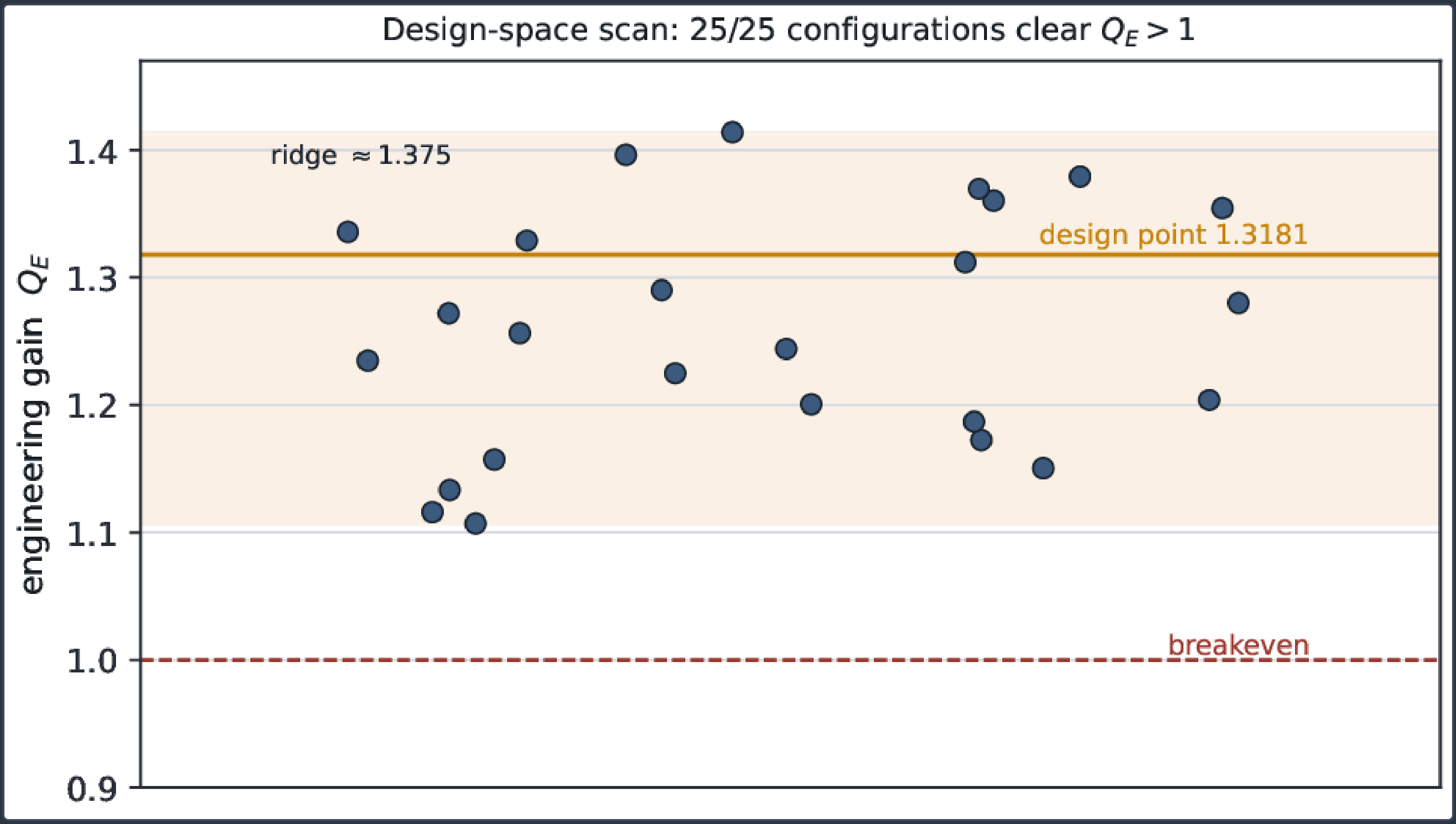

Design-space scan (data envelope; BU-L2-A2). All 25 reproduced configurations clear $Q_E > 1$, spanning $[1.107, 1.414]$ with the design point at 1.3181; intermediate points are placed within the reported envelope for display.

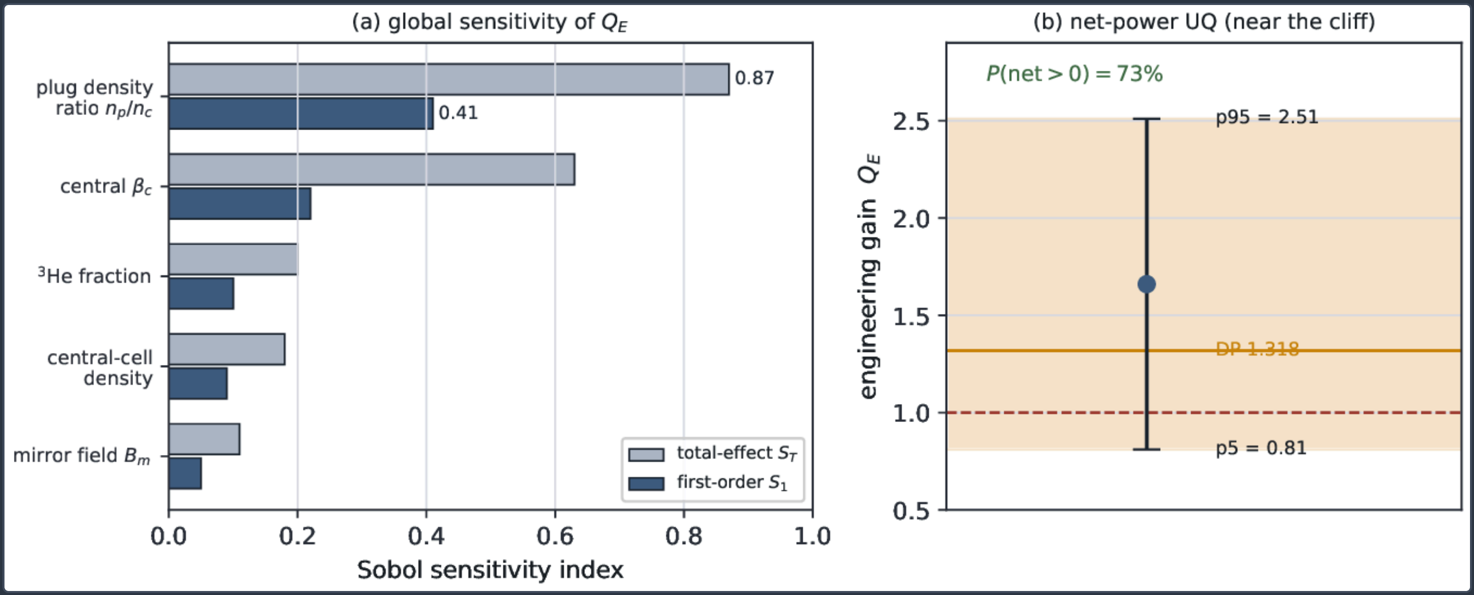

Sensitivity and net-power attribution (data; HX-05, AG-DR-02). *(a)* Sobol first-order (S_1) and total-effect (S_T) indices of Q_E: the plug density ratio dominates ($S_1 = 0.41$, $S_T = 0.87$), interacting strongly with central β_c. *(b)* Net-power Monte-Carlo band (5th–95th percentile $Q_E \in [0.81, 2.51]$) with $P(\text{net} > 0) = 73\,\%$ when the machine is placed at the cliff; the design point sits comfortably inside the band.

THE MIRROR-RATIO KNEE AND THE THERMAL-BARRIER LEVER

Two design knobs set the operating margin. The mirror ratio trades confinement against end-expander area: Q_E rises from 1.18 to 1.53 as R_{mc} goes from 3.3 to 6.8, saturating while the expander area grows roughly linearly, so the canonical $R_{\mathrm{mc}} = 4.61$ ($B_m = 17$ T on axis) sits at the practical knee (Figure 10) [AG-CX-06]. The thermal barrier is the larger lever: holding the central electron temperature near 90 keV against end-wall-cooled collapse is worth a factor of $+2.8$ in Q_E (from 0.47 to 1.318), so an electron-cyclotron-heated thermal barrier is a plug-class subsystem, not an auxiliary (Figure 11a) [AG-CX-05].

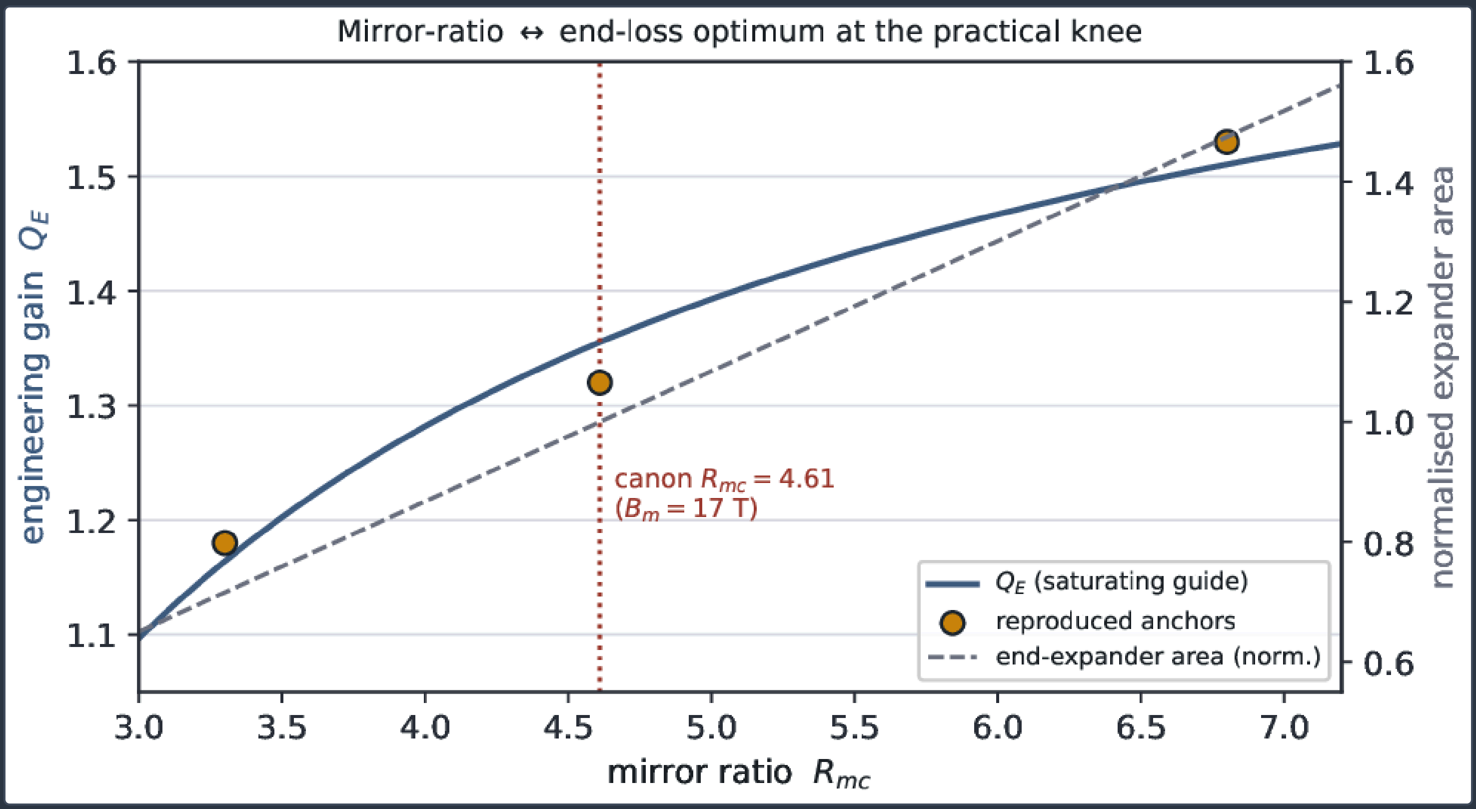

Mirror-ratio ↔ end-loss optimum (data; AG-CX-06). Reproduced anchors (markers) fit a saturating $Q_E(R_{\mathrm{mc}})$ guide (left axis); the normalised end-expander area (right axis, dashed) grows roughly linearly, placing the canonical $R_{\mathrm{mc}} = 4.61$ at the knee.

DIRECT CONVERSION IS A CONSERVATIVE FLOOR

Because most of the fusion power is charged, the electrical output is dominated by the direct converter rather than a steam cycle, so the reported gain depends on the DEC efficiency. Here the campaign is deliberately conservative. The DEC efficiency is best understood as a ladder [1,2,3]: a conservative floor of 0.56, a Moir–Barr reference value of 0.70, and an ideal proton-only ceiling of 0.85. The frozen anchor uses $\eta_{\mathrm{DEC}} = 0.49$ — *below* the floor of that ladder — and still returns $Q_E = 1.318$ (Figure 11b) [BU-SX-01]. To first order $Q_E \propto \eta_{\mathrm{DEC}}$ for the DEC-dominated output, so any realistic converter performance moves the operating point further above breakeven, not below it. The engineering gain is thus reported against a pessimistic conversion assumption: it is a floor, not a ceiling.

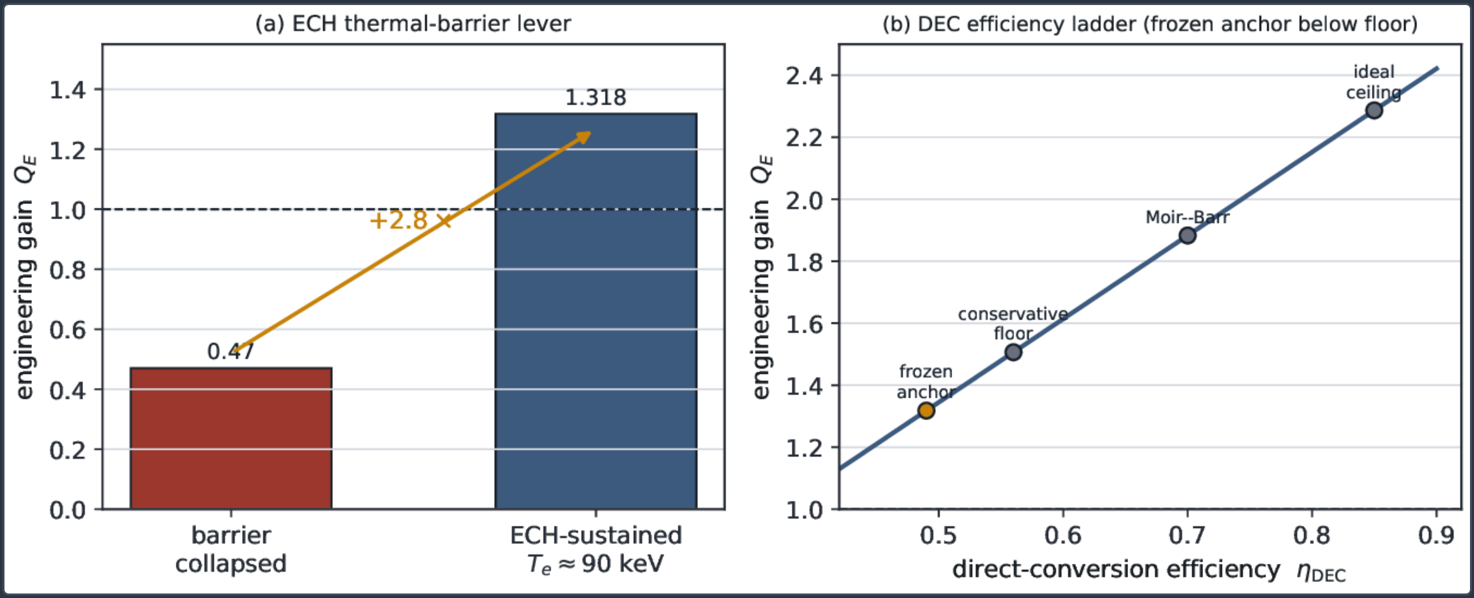

Two load-bearing levers (data). *(a)* ECH thermal-barrier lever (AG-CX-05): a sustained ~ 90 keV barrier is worth $+2.8\times$ in Q_E (from 0.47 to 1.318) relative to a collapsed barrier. *(b)* DEC efficiency ladder (BU-SX-01): the frozen anchor $\eta_{\mathrm{DEC}} = 0.49$ sits below the literature floor; the first-order scaling $Q_E \propto \eta_{\mathrm{DEC}}$ places every ladder rung above the design point.

§ 5

Discussion

The burner's power balance closes above engineering breakeven at $Q_E = 1.318$, with a genuinely low neutron fraction ($f_n = 5.44\,\%$) and a conservative conversion assumption, and the recirculating loop is resolved rather than hidden: a 2672 MWe drive returns 3522 MWe gross for $+850$ MWe net, a recirculating fraction of 0.759 that follows algebraically from $1/Q_E$. Placed against the published literature the numbers are internally consistent and externally defensible. The neutron fraction is a 15–$33\times$ reduction on a D–T anchor, exactly the advantage the D–^{3}He cycle is advertised to deliver [4,5,8]; the radiated fraction $f_{\text{rad}} = 0.592$ is squarely in the regime that Rider's non-equilibrium critique identifies as the binding constraint for advanced fuels [6,7], and the paper answers that critique concretely by naming the reflectivity that keeps the machine on the right side of it. The synchrotron model-form spread we report (AFJ vs Trubnikov differing by $\sim 2\times$, 1803 vs 919 MW) is consistent with the known uncertainty band of electron-cyclotron radiative-transfer closures [18,19,20,21], and our conservative adoption of the larger AFJ value is the pessimistic choice within that band. The confinement physics is anchored to an operating machine: reproducing WHAM's 17 T-regime Pastukhov scaling and kV-class ambipolar potential to within $\sim 5\,\%$ on fields and $\sim 6\times$ on the D–D neutron rate is a meaningful external validation for a reduced-order model [24,25,22]. Finally, the identification of the plug density ratio as the first-order variance driver ($S_1 = 0.41$) converts a favourable balance into an engineering programme: the same quantity that dominates the Sobol budget is the one carried as an explicit design requirement, so the uncertainty and the specification point at the same subsystem. The plug coil that supplies that requirement is the burner's binding magnet at 26.49 T [DOI:10.5281/zenodo.22645915; https://www.kronosfusionenergy.com/publications/engineering-the-26-49-t-plug-coil-of-a-d-he-tandem-mirr.html], a device distinct from the Hyperion breeder centrepost at 16.84 T; the two magnets are not to be conflated.

§ 6

Limitations

One gate is carried open, and it is named. The global UQ fixes the plug density and excludes central-cell radial transport, which is treated in a separate transport analysis; and the plug-to-central density ratio r_p is supplied to the balance as a requirement, $r_p = 16$, rather than solved from a first-principles plug-formation model. Equation (14) states the constraint explicitly: net gain holds down to $r_p^{\star} = 14$, so the design carries a margin $\Delta r_p = 2$, but demonstrating that the plug actually forms and holds this ratio in hardware — together with the associated first-wall reflectivity requirement $R_{\mathrm{wall}} \gtrsim 0.83$ and the assumed, not-yet-MHD-solved central $\beta_c = 0.55$ — is the load-bearing open item for the burner. It is met by a plug-formation and optical-finish specification and confirmed on a reflectivity test coupon and a plug-physics experiment; until then it is reported as a carried-open gate, not a closed result.

§ 7

Conclusion

The Kronos D–^{3}He tandem-mirror burner closes its recirculation-resolved power balance at $Q_E = 1.318$, with $P_{\rm fus} = 4298.5$ MW, $P_n = 233.95$ MW and $f_n = 5.44\,\%$ at a self-consistent $T_e = 89.72$ keV and $\varphi_i = 248.75$ keV. Resolving the plant loop gives 3522 MWe gross against a 2672 MWe recirculated drive for $+850$ MWe net, a recirculating fraction of $0.759 = 1/Q_E$. The operating point is synchrotron-limited: the correct AFJ reflective-cavity model places the machine above breakeven, an optically-thin treatment would not, and net gain requires $R_{\rm wall} \gtrsim 0.83$. The closure is robust under a $40{,}000$-sample global UQ ($P(Q_E > 1) = 1.0$) and a net-power Monte-Carlo ($P(\mathbf{net} > 0) = 73\,\%$ at the cliff), it is reported against a conservative direct-conversion efficiency of 0.49 below the literature floor, and its one open gate — the plug density ratio, with a named net-gain floor at 14 against a design value of 16 — is stated as an explicit, testable requirement. The result is a defensible, floor-not-ceiling engineering-gain closure with its controlling physics and its single open item both made explicit.

Acknowledgments tocsectionAcknowledgments Part of the Kronos Fusion Energy 2026 design series. Computation was performed on the NVIDIA GPU HPC campaign. The authors thank the Kronos physics de-risking team for the independent gate re-runs on which this paper rests.

Reproducibility tocsectionReproducibility The burner power-balance anchors ($Q_E = 1.31812$, $P_{\rm fus} = 4298.5$ MW, $P_n = 233.95$ MW, $f_n = 5.44\,\%$, $T_e = 89.72$ keV, $\varphi_i = 248.75$ keV) are frozen gates in the Kronos Physics De-Risking Register (BU-L1-A1, KX-L1-A3-BU, AG-DR-01, AG-DR-02, BU-L2-A2, KX-L1-A5-BU, HX-05, AG-CX-05, AG-CX-06, BU-SX-01, ENV-A4-BU, BV-07) and are regenerable from the frozen reduced-order mirror solver (`solve_mirror`, seed 20260726) archived with this paper. The figure-generation script (`make_pb61_figs.py`) reproduces every data figure from the tabulated anchors. This paper is archived at doi:10.5281/zenodo.22645860; official version: https://www.kronosfusionenergy.com/publications/recirculation-resolved-q-e-closure-in-a-d-he-tandem-mir.html and at its official page, https://www.kronosfusionenergy.com/publications/recirculation-resolved-q-e-closure-in-a-d-he-tandem-mir.html; the register is at doi:10.5281/zenodo.22133057.

Data availability tocsectionData availability This paper is archived at doi:10.5281/zenodo.22645860. Power-balance inputs, the synchrotron model-form sweep, the design-space scan and the uncertainty-quantification scripts are archived with the deposit and reference the Kronos 2026 series. Any economic analysis is reported separately and is not included in the public deposit.

Competing interests tocsectionCompeting interests Provisional patent applications relating to aspects of this work have been filed. The authors declare no other competing interests.

APPARATUS

Portfolio, People & Record

The intellectual-property estate, the people who built it, the limitations that gate it, and the sources it rests on.

1	4	40	27
GRANTED PATENT	2026 PROVISIONALS	TEAM MEMBERS	2022 PROVISIONALS

INTELLECTUAL PROPERTY

The patent portfolio

The estate spans a granted high-field magnet patent, pending utility and 2026 provisional filings that map to the two products, a digital-twin control provisional, a registered trademark application, and the original 2022 provisional family. Every patentable disclosure in the five-paper arXiv drop was protected **before** publication: the breeder and burner provisionals were filed 1–2 August, and a publication-gap omnibus filing the evening before the drop swept up the DEC, plasma-control, and REBCO-winding matter of the three otherwise-unprotected papers. Patent numbers and application serials are matters of public record; claim scope is summarised, not reproduced.

GRANTED & PENDING UTILITY

US 12,009,112	High-field tilted graded-REBCO magnet architecture (KRONO-002A) · *app. 17/878,550*	GRANTED
US 17/878,507	Core device / method (KRONO-001A) · *utility*	PENDING

2026 PROVISIONAL FILINGS — MAPPED TO THE PRODUCTS

64/124,209	Hyperion — spherical-tokamak tritium / helium-3 foundry · *breeder · filed Aug 2026*	FILED
64/124,220	Aegis / MetroVolt — synchrotron-cutoff, fuel-selection & plug-winding · *generator · filed Aug 2026*	FILED
64/115,167	KRONOS-CTRL digital-twin plant control · *provisional · filed Jul 2026*	FILED
64/005,440	Integrated spherical-tokamak fusion architecture · *early integrated-architecture filing · filed Mar 2026*	FILED
64/105,530	Negative-triangularity spherical-tokamak architecture · *foundational ST filing · filed Jul 2026*	FILED
64/128,097	Publication-gap omnibus — quasineutral two-species expander DEC · provenance-gated / latency-split plasma control · as-built high-field winding & conductor architecture · *filed 7 Aug 2026, the evening before the arXiv drop*	FILED

TRADEMARK & ORIGIN

FTK-98801894	Kronos Fusion Energy — trademark application	FILED
KR-2022-*	Original provisional family (KR-2022-00001 … 00027) · *27 filings, 2022*	PRIORITY

The narrow, defensible magnet novelty — the specific conductor and the digital-twin winding optimisation, not high-field REBCO as a category — is the commercial core that can earn ahead of any Q > 1 milestone, with markets in fusion magnet supply, MRI/NMR, accelerators, and proton therapy. The claim is scoped honestly: the high field is a *system field* result, not a stand-alone-coil record; the small-bore plug coil is structurally infeasible as a bare winding but resolved by a stress-managed structural shield (feasible-pending-FEA); and the winding-tape experiment returned a *null result*. The value is the method, not a field record.

THE TEAM

Founding partners, board, advisors & auditors

Kronos is built by a bench of advanced-fuel-fusion, high-field-magnet, direct-conversion, and materials specialists, with a board and operations team drawn from defense, national laboratories, and industry. Dates are shown as ranges; where a tenure has ended or is term-ending, the range says so.

FOUNDING PARTNERS — SCIENCE

Dr. Gerald Kulcinski
Co-Founder · Helium-3 & Advanced-Fuel Fusion
UW–Madison · 2023–Present

Dr. Carl Weggel
Chief Scientist / S.M.A.R.T. Design
MIT Alcator Program · 2022–Present

Dr. Robert J. Weggel
Magnetic Field Design
MIT Magnet Lab · 2022–Present

BOARD

Priyanca Ford
Founder & CEO · Executive Board
2022–Present

Bandel Carano
Finance / Strategy
Oak Investment Partners / Stanford · 2025–2026

Patrick Schweiger
Fusion Device Engineering
Oklo / CFS / TerraPower · 2025–Present

SCIENTIFIC ADVISORS

Dr. Steven O. Dean
Fusion Policy & History
DOE / Fusion Power Associates · 2025–Present

Dr. Patrick H. Diamond
Plasma Turbulence & Transport
UC San Diego · 2025–Present

Dr. Jack J. Dongarra
HPC & Numerical Algorithms
Turing Award · 2025–Present

Dr. Nasr M. Ghoniem
Chief Material Scientist
UCLA · 2025–Present

Dr. Siegfried Glenzer
Plasma Physics & Laser Fusion
Stanford / SLAC · 2022–Present

Dr. David A. Hammer
Pulsed-Power Fusion
Cornell · 2025–Present

Dr. Donald A. Spong
Plasma Theory & Confinement
ORNL · 2025–Present

Dr. Curtis Smith
Risk Assessment & Nuclear PRA
MIT / Idaho National Lab · 2025–Present

RADM (Ret.) David Goggins
Naval Engineering & Power-Plant Design
U.S. Navy · 2023–2026

Dr. Konstantin Batygin
Mathematician
Caltech · 2022–2025

Dr. Ruben Fair
Magnet Design / ITER Liaison
PPPL / Jefferson Lab · 2022–2025

Dr. Paul S. Weiss
Materials & Nanotechnology
UCLA · 2022–2025

SCIENTIFIC AUDITORS

Dr. Wilfred A. Cooper
Plasma Equilibrium Theory
EPFL / Swiss Plasma Center · 2025–Present

Dr. Ahmed Hassanein
Plasma–Material Interactions
Purdue / Argonne · 2025–Present

Dr. Patrick E. Hopkins
Extreme Thermal Materials
U. of Virginia · 2025–Present

Dr. Peter Hosemann
Materials Joining & Structural Integrity
UC Berkeley · 2025–Present

Dr. Travis W. Knight
Advanced Nuclear Fuels & Systems
U. of South Carolina · 2025–Present

Dr. Philippe Lebrun
Cryogenics & Magnet Cooling
CERN · 2025–Present

Dr. Nitendra Singh
Nuclear Safety & Fuel Cycle
ITER · 2025–Present

Dr. Guido Van Oost
Magnetic Confinement & Fusion Systems
Ghent University · 2025–Present

Dr. Gary S. Was
Radiation Materials & Structural Integrity
U. of Michigan · 2025–Present

Dr. Ray Sedwick
Direct Energy Conversion
U. of Maryland · 2025

OPERATIONS

Michael Laughlin
Chief Operating Officer
2022–Present

Martin Owens
Chief Strategy Officer
LANL / GE Hitachi · 2022–Present

MG (Ret.) Paul Pardew
Chief Contracting Officer
Army Contracting Command · 2022–Present

David Beck
Fusion Commercialization
U.S. Space Force · 2024–Present

Sushma Bhatia
Environmental & Legislative
Google · 2022–Present

Michael De Frenza
Technology Licensing
2023–Present

MG (Ret.) Robin L. Fontes
Cybersecurity & Defense
Army Cyber Command · 2022–Present

Vijay Gehani
Supply Chain & Components
INOX India · 2024–Present

Jon Michel Greenwood
IT & AI Infrastructure
Live Nation · 2023–Present

Brian C. O'Neill
National Security
CIA / ODNI · 2022–Present

Gen. (Ret.) Gustave F. Perna
DoD Liaison
Operation Warp Speed · 2022–2023

Andrea Romero
Marketing Lead
2022–Present

Legal counsel is retained; those roles are held on the internal roster and are not listed here.

SOURCES

References

1 R F Post, The magnetic mirror approach to fusion, *Nucl. Fusion* **27** 1579 (1987).

2 R W Moir and W L Barr, Venetian-blind direct energy converter for fusion reactors, *Nucl. Fusion* **13** 35 (1973). doi:10.1088/0029-5515/13/1/005

3 W L Barr and R W Moir, Test results on plasma direct converters, *Nucl. Technol./Fusion* **3** 98 (1983).

4 G L Kulcinski and J F Santarius, Advanced fuels under debate, *Nature* **396** 724 (1998).

5 J R McNally Jr, Physics of fusion fuel cycles, *Nucl. Technol./Fusion* **2** 9 (1982).

6 T H Rider, Fundamental limitations on plasma fusion systems not in thermodynamic equilibrium, *Phys. Plasmas* **4** 1039 (1997).

7 T H Rider, A general critique of inertial-electrostatic confinement fusion systems, *Phys. Plasmas* **2** 1853 (1995).

8 W M Nevins, A review of confinement requirements for advanced fuels, *J. Fusion Energy* **17** 25 (1998).

9 G I Dimov, V V Zakaidakov and M E Kishinevsky, Thermonuclear confinement with twin mirror systems, *Sov. J. Plasma Phys.* **2** 326 (1976).

10 T K Fowler and B G Logan, The tandem mirror reactor, *Comments Plasma Phys. Control. Fusion* **2** 167 (1977).

11 D E Baldwin and B G Logan, Improved tandem mirror fusion reactor, *Phys. Rev. Lett.* **43** 1318 (1979).

12 V P Pastukhov, Collisional losses of electrons from an adiabatic trap in a plasma with a positive potential, *Nucl. Fusion* **14** 3 (1974). doi:10.1088/0029-5515/14/1/001

13 R H Cohen, M E Rensink, T A Cutler and A A Mirin, Collisional loss of electrostatically confined species in a magnetic mirror, *Nucl. Fusion* **18** 1229 (1978).

14 D D Ryutov, H L Berk, B I Cohen, A W Molvik and T C Simonen, Magneto-hydrodynamically stable axisymmetric mirrors, *Phys. Plasmas* **18** 092301 (2011).

15 T C Simonen, Three game changing discoveries: a simpler fusion concept?, *J. Fusion Energy* **35** 63 (2016).

16 T K Fowler, R W Moir and T C Simonen, A new simpler way to obtain high fusion power gain in tandem mirrors, *Nucl. Fusion* **57** 056014 (2017).

17 H-S Bosch and G M Hale, Improved formulas for fusion cross-sections and thermal reactivities, *Nucl. Fusion* **32** 611 (1992).

18 A Albajar, M Bornatici and F Engelmann, Electron cyclotron radiative transfer in fusion plasmas, *Nucl. Fusion* **42** 670 (2002). doi:10.1088/0029-5515/42/6/303

19 M Bornatici, R Cano, O De Barbieri and F Engelmann, Electron cyclotron emission and absorption in fusion plasmas, *Nucl. Fusion* **23** 1153 (1983).

20 F Albajar, M Bornatici and F Engelmann, Radiation power from magnetically confined thermal plasmas, *Nucl. Fusion* **49** 115017 (2009).

21 B A Trubnikov, Universal coefficients for synchrotron emission from plasma configurations, in *Reviews of Plasma Physics* **7** 345 (Consultants Bureau, 1979).

22 P A Bagryansky *et al*, Threefold increase of the bulk electron temperature of plasma discharges in a magnetic mirror device, *Phys. Rev. Lett.* **114** 205001 (2015).

23 A A Ivanov and V V Prikhodko, Gas dynamic trap: experimental results and future prospects, *Phys.-Usp.* **60** 509 (2017).

24 D Endrizzi *et al*, Physics basis for the Wisconsin HTS Axisymmetric Mirror (WHAM), *J. Plasma Phys.* **89** 975890501 (2023).

25 J Egedal, D Endrizzi, C B Forest and T K Fowler, Fusion by beam ions in a low-collisionality, high-mirror-ratio magnetic mirror, *Nucl. Fusion* **62** 126053 (2022).

26 I M Sobol, Global sensitivity indices for nonlinear mathematical models and their Monte Carlo estimates, *Math. Comput. Simul.* **55** 271 (2001).

27 A Saltelli, Making best use of model evaluations to compute sensitivity indices, *Comput. Phys. Commun.* **145** 280 (2002).

28 J Herman and W Usher, SALib: an open-source Python library for sensitivity analysis, *J. Open Source Softw.* **2** 97 (2017).

29 P K Romano, N E Horelik, B R Herman, A G Nelson, B Forget and K Smith, OpenMC: a state-of-the-art Monte Carlo code for research and development, *Ann. Nucl. Energy* **82** 90 (2015).

30 C R Harris *et al*, Array programming with NumPy, *Nature* **585** 357 (2020).

31 P Virtanen *et al*, SciPy 1.0: fundamental algorithms for scientific computing in Python, *Nat. Methods* **17** 261 (2020).

32 J D Hunter, Matplotlib: a 2D graphics environment, *Comput. Sci. Eng.* **9** 90 (2007).

33 P I Ford, *Kronos Physics De-Risking Register*, Kronos Fusion Energy 2026 series. doi:10.5281/zenodo.22133057

COLOPHON

How this document was made

The Kronos Fleet — Combined Editorial, 2026 is set in **Fraunces** (display), **Gelasio** (text), and **IBM Plex Mono** (data & equations), carried forward from the Kronos editorial design system.

The figures are rendered at 300 dpi from the deposited generator scripts; the document is composed as a single self-contained file with embedded fonts and imagery, paginated to US Letter, and rendered to PDF through a headless Chromium engine in matched light and dark editions.

Every headline quantity carries an evidence class; withdrawn and restated values are marked as such. Nothing herein is frozen beyond the founder-approved Tier-A set.

Explore it live — turn the interactive 3-D model, run the deposited solvers in the physics validator, and watch the companion film series.

LEGAL NOTICE

Notice, status, and distribution

Conceptual design & simulation study. This document reports a conceptual design and simulation study. It is not a construction commitment, a safety-analysis report, a regulatory filing, or an offer of securities. Forward-looking statements — schedules, costs, market sizes, and performance — are estimates subject to the limitations set out in the Simulations part and may change.

Numbers and their classes. Quantities are reported with evidence classes and case labels; modelled, assumed, and requirement-class values are identified as such and are not to be quoted without their labels.

Public edition. This edition carries the physics and design only; all financial, funding, and defense-commercial content has been removed for public distribution. The scientific text corresponds to the arXiv and journal submissions.

THE 2026 KRONOS SERIES

One programme, many papers

This editorial is one paper in the Kronos 2026 series — a real fusion company's complete, reproducible physics record for a spherical-tokamak breeder and its low-neutron D–^{3}He tandem-mirror burners. Every headline number is a frozen anchor in the Physics De-Risking Register.

Explore the whole programme: the De-Risking Register, the interactive 3-D model, and the physics validator.

KRONOS FUSION ENERGY

Recirculation-Resolved Q_E Closure in a D-^{3}He Tandem-Mirror Burner: The Synchrotron-Limited Operating Point and the Carried-Open Plug Gate

A real fusion company building real machines. Explore the science, live.

Zenodo · doi:10.5281/zenodo.22645860

Read on kronosfusionenergy.com

The Physics De-Risking Register